

Machine Learning Interatomic Potentials for Million-Atom Simulations of Multicomponent Alloys

Fei Shuang,^{1,2,3,*} Penghua Ying,^{4,†} Kai Liu,² Zixiong Wei,² Fengxian Liu,³ Zheyong Fan,⁵ Minqiang Jiang,^{1,6} and Poulumi Dey^{2,‡}

¹*State Key Laboratory of Nonlinear Mechanics, Institute of Mechanics, Chinese Academy of Sciences, Beijing, China*

²*Department of Materials Science and Engineering, Faculty of Mechanical Engineering, Delft University of Technology, Mekelweg 2, 2628 CD Delft, the Netherlands*

³*Faculty of Engineering Technology, University of Twente, Drienerlolaan 5, 7522NB Enschede, the Netherlands*

⁴*Laboratory for multiscale mechanics and medical science, SV LAB,*

School of Aerospace, Xi'an Jiaotong University, Xi'an, Shaanxi, 710049, China

⁵*College of Physical Science and Technology, Bohai University, Jinzhou 121013, China*

⁶*School of Engineering Science, University of Chinese Academy of Sciences, Beijing, China*

(Dated: April 3, 2026)

Machine learning interatomic potentials (MLIPs) with broad chemical flexibility are important for atomistic simulations of compositionally complex materials such as high-entropy alloys. Here, we study two state-of-the-art MLIP frameworks, the neuroevolution potential (NEP) and the graph atomic cluster expansion (GRACE), for 16 elemental metals and multicomponent alloys. GRACE potential with Finnis–Sinclair type shows substantially higher training efficiency and consistently, though only slightly, better accuracy for mechanical properties, thermal stability, and chemical extrapolation. In contrast, NEP achieves an approximately 60-fold higher inference speed, making it attractive for million-atom molecular dynamics simulations. We further examine uncertainty quantification strategies and find that ensemble-based uncertainty correlates robustly with model error, whereas D-optimality is less reliable for the systems considered here. Large-scale nonequilibrium molecular dynamics simulations of shock propagation further show that NEP, combined with ensemble-based uncertainty quantification, enables efficient and reliable simulations under extreme dynamic conditions.

Keywords: Neuroevolution potential, graph atomic cluster expansion potential, metals and alloys

INTRODUCTION

Machine learning interatomic potentials (MLIPs) have transformed atomistic modelling across metals, alloys [1], and complex inorganic materials [2]. Foundational developments began with Behler–Parrinello-type neural network potentials (NNPs) [3] and Gaussian Approximation Potentials (GAP) [4], and were subsequently extended by several influential frameworks, including the Spectral Neighbor Analysis Potential (SNAP) based on bispectrum descriptors, Moment Tensor Potentials (MTPs) as a systematically improvable polynomial formalism [5], Deep Potential for scalable deep-learning-based force fields, and the Atomic Cluster Expansion (ACE) as a systematically organized body-order expansion [6]. More recently, pretrained or universal MLIPs, such as MACE [7], CHGNet [8], eqV2 [9], SevenNet [10], and Orb [11], have further expanded elemental coverage and improved transferability across broad classes of materials. These advances have substantially improved both accuracy and generality. However, many universal mod-

els rely on computationally intensive equivariant graph or message-passing architectures, which can make routine long-timescale molecular dynamics (MD) at very large scales considerably more demanding than with lighter-weight MLIP frameworks. As a result, despite their broad applicability and strong predictive performance, current demonstrations of such models have remained focused predominantly on molecular systems or materials simulations at moderate system sizes, typically up to the order of tens of thousands of atoms [12, 13].

Within this landscape, neuroevolution potential (NEP) [14] offers a compact GPU-native route to balancing accuracy and throughput. NEP builds radial and angular bases from Chebyshev and Legendre polynomials, couples them to shallow neural networks, and trains with natural evolution strategies in GPUMD [15]. The design favors simple kernels, coalesced memory access, and low-latency evaluation, enabling very high atom-step rates on data-center and commodity GPUs. NEP has been used for million-atom heat-transport simulations [16] and efficient path-integral MD [17] while remaining close to first-principles fidelity. More recently, a universal variant, NEP89, has been introduced for inorganic and organic materials across 89 elements, delivering the same computational efficiency for million-atom simulations [18].

Graph atomic cluster expansion (GRACE) is a recently developed MLIP framework tailored for chemically

* These authors contributed equally to this work.; shuangfei@imech.ac.cn

† These authors contributed equally to this work.

‡ P.Dey@tudelft.nl

complex and multicomponent systems [19]. GRACE extends the ACE formalism by introducing graph-based basis functions that capture semi-local interactions while preserving permutation, translation, and rotation invariances. Recent work has trained foundational GRACE models on some of the largest available materials datasets (MPtrj [8], OMat24 [20] and Alexandria [21]), reporting a new Pareto frontier between accuracy and per-atom computational cost [22]. In particular, the Finnis–Sinclair-type variant (GRACE-FS) is highlighted for its straightforward parallelization and capability for efficient CPU-only inference, with reported timings indicating favourable scaling in LAMMPS [23].

This context motivates a more practical question for metals and alloys: which MLIP frameworks can simultaneously provide broad elemental scalability and genuine feasibility for extreme-scale MD? In this regard, NEP and GRACE-FS are particularly noteworthy. Unlike many current universal MLIPs, which are primarily demonstrated at system sizes up to tens of thousands of atoms, both NEP and GRACE-FS are designed in a way that makes million-atom simulations a realistic target. NEP has already shown this capability in large-scale simulations via GPUMD, while GRACE-FS has emerged as a promising alternative with a distinct algorithmic design, favourable scaling, and efficient large-scale inference. A direct and protocol-consistent comparison between NEP and GRACE-FS is therefore especially timely. Such a comparison is important not only for clarifying their relative strengths in accuracy, efficiency, stability, and extrapolation, but also for identifying what is required for MLIPs to move beyond general-purpose accuracy and toward production-scale simulations of compositionally complex materials.

The scientific payoff is immediate for high-entropy materials, where chemically frustrated disorder and multi-scale microstructures demand very large simulation volumes. High-entropy alloys benefit from supercells that capture short-range order, clustering, dislocation networks, and grain boundaries, often at scales beyond thousands of atoms [24–26]. High-entropy two-dimensional materials [27] and high-entropy ceramics [28] similarly require both wide elemental coverage and large-scale simulations to probe phase stability, defect thermodynamics, and transport. Related extreme-scale arenas include additive-manufacturing thermal cycles, shock and impact loading, radiation damage cascades, and nanocrystalline grain growth, where million-atom domains are commonly reported or strongly indicated [29, 30].

Against this backdrop, we present a comparative study of NEP and GRACE-FS trained on a chemically diverse dataset covering 16 elemental metals and their representative alloys. We first evaluate their predictive accuracy on training and test sets, together with finite-temperature stability and computational efficiency. We then examine the applicability of two uncertainty quan-

tification approaches for these models. To assess extrapolation behaviour, we systematically analyse how prediction errors evolve with increasing chemical complexity. In addition, both models are validated against a range of physics-grounded properties, including elastic constants, defect energetics, and deformation responses. Finally, leveraging its superior computational efficiency, we employ NEP to perform a three-million-atom shock simulation of a high-entropy alloy and analyse the associated uncertainties.

MATERIALS AND METHODS

Training and test datasets

The datasets used in this work consist of three components. First, the training dataset is taken from Ref. [31], which covers 16 metallic elements (Ag, Al, Au, Cr, Cu, Mg, Mo, Ni, Pb, Pd, Pt, Ta, Ti, V, W, Zr) and includes only configurations of pure metals and binary alloys.

Second, we follow the testing protocol of Ref. [31], which evaluates model transferability using public multicomponent datasets that extend well beyond the unary and binary training domain. In particular, Song et al. assessed force predictions on three independent datasets containing 3-component, 4-component, and even up-to-13-component structures, and further examined formation energies using ternary Materials Project structures and GNoME structures ranging from 2 to 5 components. These test data therefore provide a substantially broader benchmark for evaluating model accuracy outside the training distribution.

Third, to systematically probe chemical transferability, we construct an additional benchmark dataset of multicomponent alloys covering all compositional orders from 2 to 16 elements. The dataset contains 800 structures in total, spanning the 8 possible levels of compositional complexity. For each order, structures are generated with randomized elemental selections, concentrations, and atomic arrangements, with the goal of covering as many distinct elemental combinations as possible rather than exhaustively enumerating the full combinatorial space. This design provides a systematic benchmark for evaluating how model performance changes as the chemical complexity increases from binary to highly multicomponent alloys. All structures are evaluated using density functional theory (DFT) calculations.

DFT calculations

DFT calculations are performed for all newly generated configurations using the Vienna *ab initio* simulation package (VASP) [32]. The exchange–correlation interactions are described by the Perdew–Burke–Ernzerhof

(PBE) functional [33], and electron–ion interactions are treated using the projector-augmented-wave (PAW) method [34]. An energy convergence criterion of 10^{-6} eV is used for electronic self-consistency. The plane-wave cutoff energy is set to 520 eV. Brillouin zone sampling is performed using Monkhorst–Pack grids generated by VASPKIT [35], with a consistent reciprocal-space density of $2\pi \times 0.03 \text{ \AA}^{-1}$.

Neuroevolution potential

The NEP models used in this work are identical to the UNEP-v1 model ensemble reported in Ref. [31]. All UNEP-v1 models and corresponding reference datasets have been previously deposited in the Zenodo repository <https://doi.org/10.5281/zenodo.11533864> [36].

The UNEP-v1 models were trained using the NEP4 architecture [31] implemented in the GPUMD package [15] to represent 16 elemental metals and their alloys. In this framework, the total energy is decomposed into site energies as $U = \sum_{i=1}^N U^i$. Specifically, NEP4 maps a descriptor vector \mathbf{q}^i of a central atom i to its site energy U^i using species-dependent neural network (NN) parameters \mathbf{w}^I (collectively denotes the weight and bias parameters) for each atom type I :

$$U^i = \sum_{\mu=1}^{N_{\text{neu}}} w_{\mu,I}^{(1)} \tanh \left(\sum_{\nu=1}^{N_{\text{des}}} w_{\mu\nu,I}^{(0)} q_{\nu}^i - b_{\mu,I}^{(0)} \right) - b_I^{(1)}, \quad (1)$$

which can be formally expressed as $U^i = \mathcal{N}(\mathbf{w}^I; \mathbf{q}^i)$. Notably, while using species-dependent parameters increases the total number of trainable parameters, it does not significantly increase the computational cost during MD simulations because it only involves a selection of the correct set of NN parameters for a given atom [31].

The training setup of UNEP-v1 utilized descriptor cutoffs of 6 Å for radial components and 5 Å for angular components, with angular terms extending up to five-body interactions. The descriptors \mathbf{q}^i are constructed from radial functions $g_n(r_{ij}) = \sum_k c_{nk}^{I,J} f_k(r_{ij})$, where the expansion coefficients $c_{nk}^{I,J}$ are also trainable parameters specific to the atom pairs (I, J) .

These descriptors were constructed using 5 radial functions expanded via 9 basis functions for both radial and angular parts. The regression model for each species employed a feedforward neural network with a single hidden layer containing 80 neurons, resulting in a 35-80-1 architecture per element. To accurately handle high-energy short-range interactions, a Ziegler-Biersack-Littmark (ZBL) potential [37] with a 2 Å cutoff was incorporated into the potential.

Beyond the primary model, the UNEP-v1 release includes an ensemble of 8 separate models. These were generated by systematically varying the hyperparameters, including the number of radial functions and the

number of neurons in the hidden layer (see Ref. [36] for details), within the UNEP-v1 training input to ensure statistical robustness and facilitate uncertainty estimation across the chemical space of the 16 elemental metals and their diverse alloys.

Graph atomic cluster expansion potential

The GRACE potential is the extension of the ACE potential. In the ACE formulation, the energy of the system of N atoms is decomposed into atomic contributions as $E = \sum_i E_i$, where $i = 1, \dots, N$. For each contribution, it is represented by a function \mathcal{F} of P atomic properties:

$$E_i = \mathcal{F}(\varphi_i^{(1)}, \dots, \varphi_i^{(P)}). \quad (2)$$

The atomic property has the form:

$$\varphi_i^{(p)} = \sum_{\nu} c_{\nu}^{(p)} \mathbf{B}_{i\nu}, \quad (3)$$

where $c_{\nu}^{(p)}$ is the expansion coefficients and $\mathbf{B}_{i\nu}$ is the basis functions. Generally, the function \mathcal{F} is a nonlinear function, for example in the form of generalized Finnis-Sinclair potential

$$E_i = \varphi_i^{(1)} + \sqrt{\varphi_i^{(2)}}. \quad (4)$$

However, in the GRACE formulation, the decomposition of the system energy is not performed in the beginning. First, the system energy is expressed as $E = E(\boldsymbol{\sigma})$, where $\boldsymbol{\sigma} = (\mathbf{r}_1, \mu_1, \dots, \mathbf{r}_N, \mu_N)$ is the configuration depending on the atomic positions \mathbf{r}_i and atom properties μ_i such as the species or magnetic moments. After attaching single-particle basis functions to each atom, the cluster basis functions $\Phi_{\alpha\nu}$ are obtained from their products. Thereby, the system energy is represented by the linear combination of the cluster basis functions

$$E = \sum_{\alpha\nu} J_{\alpha\nu} \Phi_{\alpha\nu}(\boldsymbol{\sigma}), \quad (5)$$

where $J_{\alpha\nu}$ is the expansion coefficients. Then, the graph topology of the configuration is considered for the simplifications of the cluster basis functions. Specifically, the clusters in the configuration are either star or tree graphs, where directed edges and nodes correspond to bonds and atoms, respectively. To resemble the decomposition of system energy into atomic contributions, the contribution of the graph-based cluster basis functions is assigned to the root nodes, leading to the introduction of atomic bases in the functional form of single-particle basis functions. Next, the tree graphs are decomposed into star graphs on different layers from the root node. In this way, local ACE potentials could be defined on different layers so that the GRACE potential are evaluated in

a recursive approach. Finally, the atomic contributions could be written as

$$E_i = \sum_k \lambda_k^{(\mu_i)} \varphi_{ik}^{(0)}, \quad (6)$$

where $\varphi_{ik}^{(0)}$ is local ACE potential.

Notably, compared to the ACE potential, the GRACE potential doesn't have the limit on the number of elements to be parameterized. This is due to the modification of its radial basis function to include pairwise chemical dependence, resulting in the vanishing of the chemical index into the entries of the expansion coefficients. In addition, GRACE models of different complexities are used in this study, namely GRACE-FS, GRACE-1L, and GRACE-2L. The difference between them is in the range of the message passing. Specifically, the GRACE-FS model is similar to Finnis-Sinclair-type ACE model but with chemical embedding to parameterize unlimited number of elements, while GRACE-1L and GRACE-2L represent one-layer and two-layer models, respectively.

In this study, we employ the GRACE-FS framework to train MLIP models with different levels of complexity, quantified by their parameter counts. Following the *gracemaker* definitions [19], we consider small, medium, and large variants, denoted as GRACE-FS-S, GRACE-FS-M, and GRACE-FS-L, respectively. To further probe the role of architectural design, we additionally train a more complex graph-based model, GRACE-2L, within the same GRACE framework. A uniform cutoff radius of 6 Å is adopted for all models. Beyond the primary model, we also train 10 additional GRACE-FS-M models for high-quality uncertainty quantification.

Uncertainty quantification

We use ensemble learning and D-optimality to estimate the prediction errors of our MLIPs on unseen atomic configurations. The ensemble method quantifies uncertainty using the variance in force predictions across multiple models [38]. Additionally, we use D-optimality with the MaxVol algorithm [39] to compute an extrapolation grade for structures relative to the reference dataset.

Ensemble-based uncertainty quantification is applied to both the UNEP-v1 and GRACE-FS models, with 8 models used for each case. For D-optimality based uncertainty quantification, NEP tool sets [40] gives out-of-memory errors on 16-element dataset (>100,000 structures). Therefore it is only applied to GRACE-FS models with *gracemaker*.

Following Ref. [38], we define the estimated uncertainties for individual atoms ($U_{F,\text{atom}}$) and entire configurations ($U_{E,\text{cfg}}$, $U_{F,\text{cfg}}$) as the maximum deviations across the ensemble:

$$U_{E,\text{cfg}} = \max_k |E_j^k - \langle E_j \rangle|, \quad (7)$$

$$U_{F,\text{atom}} = \max_k |\mathbf{F}_i^k - \langle \mathbf{F}_i \rangle|, \quad (8)$$

$$U_{F,\text{cfg}} = \max_{i \in j} (\max_k |\mathbf{F}_i^k - \langle \mathbf{F}_i \rangle|), \quad (9)$$

where $k = 1, \dots, K$ indices the MLIP models, E_j^k and \mathbf{F}_i^k are the individual model predictions, and $\langle E_j \rangle$ and $\langle \mathbf{F}_i \rangle$ are the ensemble averages. We compare these uncertainties to their respective ground-truth DFT errors:

$$e_{E,\text{cfg}} = |E_j^{\text{DFT}} - \langle E_j \rangle|, \quad (10)$$

$$e_{F,\text{atom}} = |\mathbf{F}_i^{\text{DFT}} - \langle \mathbf{F}_i \rangle|, \quad (11)$$

$$e_{F,\text{cfg}} = \max_{i \in j} |\mathbf{F}_i^{\text{DFT}} - \langle \mathbf{F}_i \rangle|. \quad (12)$$

Simulation and visualization packages

LAMMPS [23] and GPUMD [15] are used for large-scale MD simulations. To evaluate the computational efficiency of the new GPUMD version, we perform inference speed tests using and GPUMD-v5.0. OVITO is employed for the visualization and analysis of atomic structures [41].

RESULTS

Training performance of MLIPs

We begin by comparing the training performance of UNEP-v1 and GRACE-FS-M in Fig. 1. The error distributions for energy, force, and stress in Fig. 1(a-c) are broadly similar for the two models. GRACE-FS-M shows a slightly heavier tail in the force distribution and more pronounced high-error tails for energy and stress. In terms of mean absolute error (MAE), GRACE-FS-M yields slightly lower errors for energy (10.42 meV/atom) and force (99.11 meV/Å) than UNEP-v1 (11.10 meV/atom and 111.08 meV/Å, respectively), whereas UNEP-v1 gives a lower stress MAE (0.45 GPa versus 0.51 GPa). The root-mean-square errors (RMSEs) show a similar overall trend for force, with GRACE-FS-M again slightly outperforming NEP (159.14 versus 171.90 meV/Å), but they also reflect the stronger sensitivity of RMSE to the high-error tails: for energy and stress, the RMSEs of GRACE-FS-M (21.02 meV/atom and 2.52 GPa) exceed those of UNEP-v1 (17.13 meV/atom and 1.18 GPa), consistent with the broader tails in the corresponding error distributions. Overall, the two models exhibit comparable training accuracy, with GRACE-FS-M performing slightly better in the average energy and force errors, and UNEP-v1 showing better robustness against large energy and stress outliers.

Training efficiency shows a much sharper contrast. As shown in Fig. 1(d), UNEP-v1 required ten days on four A100 GPUs to complete 1,000,000 generations [31], whereas GRACE-FS-M converged within one day on a single A100 GPU in fewer than 2,000 epochs. This corresponds to an approximately 40-fold reduction in training wall time, highlighting a major practical advantage of GRACE-FS-M for model development and iteration.

To examine the effect of model complexity, we further consider GRACE-FS-S, GRACE-FS-L, and the two-layer graph-based model GRACE-2L. The numbers of parameters and training errors are listed in Table I, and the corresponding test errors are given in Table II. The test set from Ref. [31] contains pure metals and alloys under diverse deformation states. All GRACE-FS models contain fewer parameters than UNEP-v1, whereas GRACE-2L is substantially larger.

For all models, the energy errors on the test set are higher than those on the training set, indicating a clear generalization gap. This trend is seen in both MAE and RMSE, suggesting not only a shift in the average prediction error but also a deterioration in the larger-error regime on unseen configurations. This suggests that training only on pure metals and binary alloys is insufficient to fully represent the more complex chemical environments in the test set. Within the GRACE-FS series, increasing model size leads to modest reductions in both MAEs and RMSEs for energy and force, with smaller changes for stress. GRACE-FS-M and GRACE-FS-L both outperform UNEP-v1 in the MAEs of energy and force on the training and test sets, whereas NEP yields somewhat lower stress MAEs than all GRACE-FS variants. A similar trend is observed for the force RMSE, for which GRACE-FS-M and GRACE-FS-L remain lower than UNEP-v1. By contrast, for energy and

stress, the RMSEs of the GRACE-FS models are not uniformly lower than those of UNEP-v1, indicating that although GRACE-FS improves the average predictive accuracy, UNEP-v1 remains more robust to a subset of larger errors in these quantities.

GRACE-2L achieves substantially lower MAEs for all three target properties, especially on the test set, indicating the benefit of increased model expressivity and a more flexible graph-based message-passing architecture. Its RMSEs are also generally reduced for energy and force relative to UNEP-v1 and the GRACE-FS models, supporting improved overall transferability, although the stress RMSE remains comparatively high on the training set, suggesting that a small number of large stress errors still persist. However, its parameter count is more than an order of magnitude larger than that of UNEP-v1 and far exceeds those of the GRACE-FS models. Since the primary goal of this work is to compare UNEP-v1 and GRACE-FS as practically deployable MLIPs for chemically complex, large-scale simulations, the most relevant conclusion is that GRACE-FS provides slightly better average accuracy for energy and force than UNEP-v1, whereas UNEP-v1 retains an advantage in stress prediction and in limiting some large energy and stress outliers.

Uncertainty quantification

We next examine the uncertainty of the two MLIPs using ensemble learning and D-optimality approaches. The test dataset from Ref. [31] is used for the uncertainty quantification (UQ) analysis. The Spearman’s correlation (ρ) is used to measure the quality of UQ analysis. Fig. 2(a-d) show that using ensemble discrepancies of UNEP-v1 and GRACE-FS-M models can give good estimation of errors for unknown atomic environments. GRACE-FS ensembles exhibit the higher correlation than UNEP-v1 ensembles, potentially because the UNEP-v1 utilize varying model sizes while GRACE-FS-M maintains consistency across models. Notably, for both UNEP-v1 and GRACE-FS-M ensembles, the correlation between force error and UQ is stronger when evaluated on a per-structure basis (Fig. 2(b) and (d)) than on a per-atom basis (Fig. 2(a) and (c)).

In contrast, the D-optimality results shown in Fig. 2(e, f) exhibit a poor correlation between force errors and γ values at both the structural and atomic levels. In particular, the commonly used threshold of $\gamma = 1$ fails to reliably distinguish atoms or structures associated with low prediction errors, indicating that D-optimality is not a robust metric for quantifying uncertainty in previously unseen local atomic environments (LAEs), either in active-learning workflows or in single-shot prediction scenarios.

This failure of D-optimality is consistent with our recent findings on the impact of data heterogeneity on uncertainty quantification [42]. In the present dataset, both

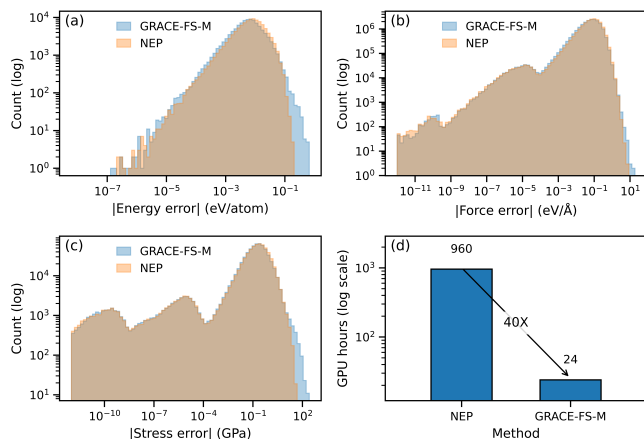


FIG. 1. Benchmarking the accuracy and efficiency of UNEP-v1 and GRACE-FS-M potentials. Error distributions for (a) energy, (b) forces, and (c) virial stress are compared alongside (d) the computational cost (wall time) required for training.

TABLE I. Mean absolute errors (MAE) and root-mean-square errors (RMSE) of energy (E), force (F), and stress (S) for different MLIPs on the training set.

MLIPs	UNEP-v1	GRACE-FS-S	GRACE-FS-M	GRACE-FS-L	GRACE-2L
# of Parameters	70,401	9,312	17,824	28,592	1,289,704
E_{MAE} (meV/atom)	11.10	11.81	10.42	9.30	3.29
E_{RMSE} (meV/atom)	17.13	23.75	21.02	18.93	14.09
F_{MAE} (meV/Å)	111.08	103.85	99.11	95.95	55.15
F_{RMSE} (meV/Å)	171.90	168.59	159.14	153.73	88.15
S_{MAE} (GPa)	0.45	0.53	0.51	0.50	0.35
S_{RMSE} (GPa)	1.18	2.46	2.52	2.64	4.74

TABLE II. Mean absolute errors (MAE) and root-mean-square errors (RMSE) of energy (E), force (F), and stress (S) for different MLIPs on the test set from Ref. [31].

MLIPs	UNEP-v1	GRACE-FS-S	GRACE-FS-M	GRACE-FS-L	GRACE-2L
E_{MAE} (meV/atom)	24.44	20.07	19.89	18.94	11.54
E_{RMSE} (meV/atom)	57.99	62.97	55.85	68.00	64.61
F_{MAE} (meV/Å)	114.24	102.13	98.98	95.23	62.00
F_{RMSE} (meV/Å)	260.09	424.51	408.41	457.09	334.00
S_{MAE} (GPa)	0.67	0.65	0.62	0.61	0.37
S_{RMSE} (GPa)	2.13	3.07	2.47	2.86	2.18

structural and chemical diversity are substantial: the training set includes configurations associated with severe plastic deformation and free surfaces, and spans 16 elements together with their binary alloys. Under such conditions, D-optimality mainly characterizes the outer boundary of the sampled descriptor space. As a result, although the overall boundary of the training set may appear sufficiently broad, critical novel structures located within sparsely sampled or internally underrepresented regions can still be missed. These structurally important yet inadequately represented configurations are therefore not effectively identified by D-optimality.

Computational efficiency cross different scales

We next evaluate the computational efficiency of the MLIPs, which is critical for enabling extra-large-scale MD simulations. The performance of UNEP-v1 is benchmarked on both GPU (NVIDIA H100 and A100) and CPU platforms on the Snellius cluster, the national supercomputer of the Netherlands. CPU calculations are carried out on a dual-socket system equipped with AMD EPYC 9654 processors (192 cores in total).

For a fair comparison with the CPU-only GRACE-FS-M model, all CPU benchmarks are performed using 192 cores. This configuration is chosen to match the computational cost of approximately one H100 GPU-hour on the Snellius system, where CPU and GPU nodes are charged at comparable rates. The resulting performance comparison therefore reflects a cost-normalized evaluation rather than a direct hardware-to-hardware comparison.

The results, summarized in Fig. 3, demonstrate a substantial performance advantage for the GPU-accelerated UNEP-v1 over the CPU-based GRACE-FS-M model. For pure Cu, the H100 GPU reaches a peak inference speed of 29.4 million atoms per step per second (Matom-step/s) at 2.05 million atoms, compared with 0.503 Matom-step/s for GRACE-FS-M on 192 CPU cores, corresponding to a speedup of about $58\times$. At the same system size, the A100 achieves 15.4 Matom-step/s, which is still more than $30\times$ faster than the CPU reference. For the chemically more complex $\text{Al}_{31}\text{Cr}_6\text{Cu}_{22}\text{Ni}_{32}\text{V}_9$ HEA, the H100 attains a peak speed of 19.7 Matom-step/s at 256 thousand atoms, whereas GRACE-FS-M reaches 0.571 Matom-step/s, yielding a speedup of about $34\times$. The A100 reaches 10.6 Matom-step/s for the same HEA system, maintaining a clear advantage over the CPU-based model.

The scaling behavior of the two platforms also differs significantly. While the CPU performance of GRACE-FS-M is largely system-size agnostic over the tested range, the GPU computational efficiency of UNEP-v1 improves substantially with increasing system size and reaches peak throughput for systems containing hundreds of thousands to millions of atoms. This behavior is characteristic of GPU architectures, where parallelization overhead is progressively amortized at larger system sizes, making UNEP-v1 particularly well suited for extra-large-scale molecular dynamics simulations. A direct comparison between GPUs further shows that the H100 is consistently faster than the A100, with an advantage of about $1.74\text{--}1.91\times$ for Cu and $1.81\text{--}1.99\times$ for the HEA, depending on system size. Given that the H100 is

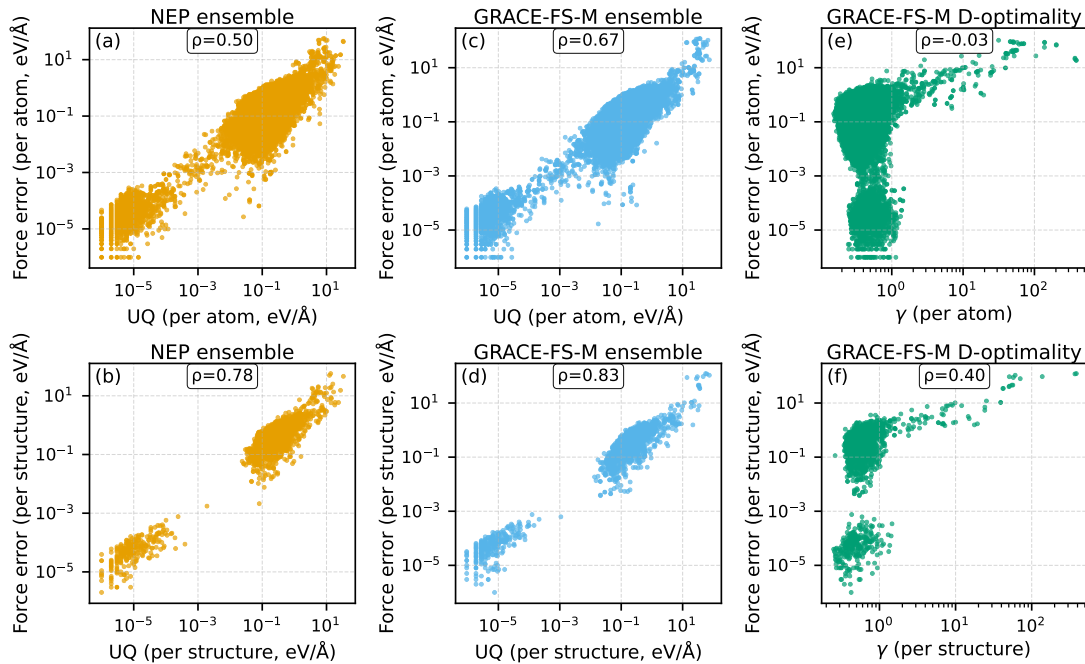


FIG. 2. Uncertainty quantification for UNEP-v1 and GRACE-FS-M potentials. (a, b) Uncertainty estimates for UNEP-v1 using ensemble learning at the atomic and structural levels, respectively. (c-f) Uncertainty estimates for GRACE-FS-M using (c, d) ensemble learning and (e, f) the D-optimality criterion, each shown at the atomic and structural level.

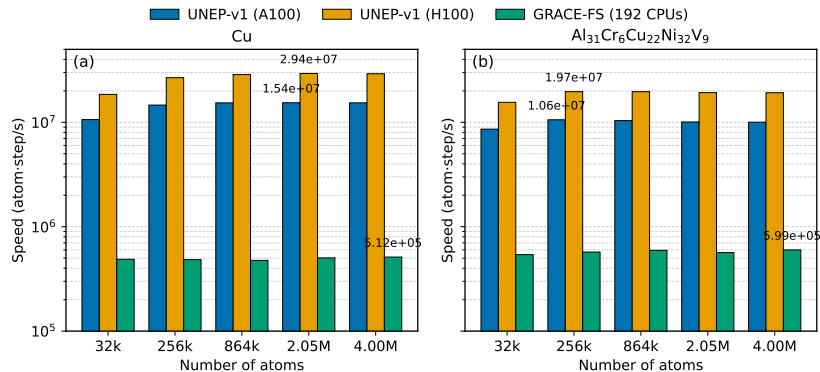


FIG. 3. Computational speed comparison between UNEP-v1 and GRACE-FS-M for (a) pure Cu and (b) the $\text{Al}_{31}\text{Cr}_6\text{Cu}_{22}\text{Ni}_{32}\text{V}_9$ HEA. UNEP-v1 is evaluated on A100 and H100 GPUs, while GRACE-FS-M is run on 192 CPU cores.

only about $1.5\times$ more expensive than the A100 on the Snellius cluster, it also delivers a superior performance-to-cost ratio. Therefore, the combination of UNEP-v1 accelerated on an H100 GPU emerges as the most powerful and cost-effective computational pathway for extra-large-scale MD simulations of complex material systems in this work.

MD Simulation stability

We evaluate the stability of two MLIPs in MD simulations under different temperatures by adapting the procedure from Ref. [43]. For a given system, we con-

duct an NVT simulation for 10 ps with a specific initial temperature followed by a 100 ps NVE simulation, monitoring the total energy drift during the NVE phase. A non-zero energy drift reflects numerical inaccuracies inherent to the potential, as the total energy should be conserved in an NVE ensemble. The results for monolayer goldene are presented in Fig. 4. Both MLIPs exhibit a similar, temperature-dependent energy drift, with all values remaining below 2.5×10^{-3} meV/atom (Fig. 4a). Despite this quantitative similarity in energy conservation, a critical qualitative difference in structural stability is observed. As shown in Fig. 4(b, c), the goldene structure remains stable as a monolayer when simulated with the UNEP-v1 potential. In contrast, the structure

collapses into a thicker, multi-layer configuration when simulated with the GRACE-FS-M potential. This divergence indicates that the two MLIPs impart different thermal stability to the goldene monolayer. Nevertheless, both potentials successfully maintain the atomic coordination of gold, confirming their ability to model metallic systems without catastrophic failure.

We next assess the MLIPs on more complex multi-component systems to evaluate their robustness. The first case is the quinary alloy $\text{Al}_{31}\text{Cr}_6\text{Cu}_{22}\text{Ni}_{32}\text{V}_9$, a system previously studied for its short-range order (SRO) formation [31]. Using the SRO-containing structure from this prior work as a starting point, we evaluated the stability of the MLIPs. As shown in Fig. 5(a), GRACE-FS-M and UNEP-v1 demonstrate comparable energy drift up to 2,000 K. However, at 3,000 K, the UNEP-v1 model exhibits an abrupt energy jump, which is two orders of magnitude larger than that of GRACE-FS-M, indicating a catastrophic numerical instability at this extreme temperature and clearly demonstrating the superior high-temperature stability of GRACE-FS-M. We further probe the limits of both potentials using a high-entropy alloy comprising all 16 elements (Fig. 5(b)). Here, the two models perform similarly up to 1,000 K. At elevated temperatures of 2,000 K and 3,000 K, however, UNEP-v1 again shows a significantly higher energy drift than GRACE-FS-M, reinforcing the performance gap observed in the quinary system. A key observation is that for both MLIPs, the energy drifts in these multi-element alloys are substantially higher than those observed in the pure goldene system (Fig. 4), highlighting the increased challenge of conserving energy in chemically complex environments.

These results collectively underscore a critical trend: as compositional complexity and simulated temperature increase, the architectural advantages of the GRACE-FS-M potential become increasingly pronounced. While both potentials are stable under moderate conditions, UNEP-v1 fails at the thermodynamic extremes, particularly in multi-component systems where its errors

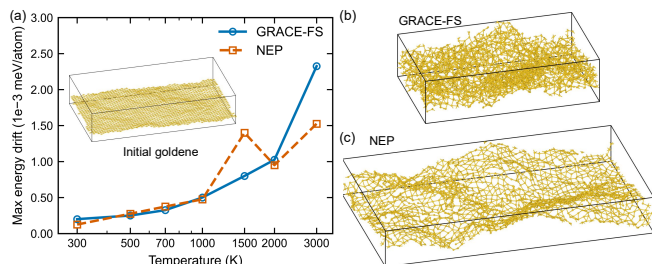


FIG. 4. Thermal stability of goldene assessed by MD simulations. (a) Maximum energy drift as a function of temperature. (b, c) Atomic snapshots of the structure after relaxation at 1,500 K, showing the different structures obtained by two MLIPs at extreme conditions.

are substantially larger. This conclusively shows that GRACE-FS-M provides more reliable and stable MD simulations for complex alloys, especially under demanding conditions.

Transferability of MLIPs and augmented GRACE-FS

The applicability of MLIPs to multicomponent alloys remains a critical open question, as current models are trained exclusively on unary and binary systems. To systematically assess and compare the accuracy of leading MLIPs, we introduce a novel benchmark dataset designed for maximum compositional diversity. This dataset comprises eight distinct systems, ranging from 2 to 16 elements. For each system size, we generated 100 random configurations with varying elemental compositions and atomic perturbations. The performance of each potential is evaluated by comparing its predictions against high-fidelity, single-point DFT calculations.

Fig. 6 presents a comparative analysis of the UNEP-v1, GRACE-FS-M, and GRACE-2L models, revealing a definitive performance hierarchy: GRACE-2L is the most accurate, followed by GRACE-FS-M, with UNEP-v1 exhibiting the highest errors. This result is striking because all models are trained on datasets containing only unary and binary systems, yet they generalize to multicomponent environments with vastly different success. This immediately suggests a profound dependence on model architecture. To quantitatively investigate this architectural dependence, we trained an augmented model, GRACE-FS-M-A, by supplementing the original training data with our newly generated multi-component structures. These newly generated datasets span configurations ranging from 2 to 16 elements, reflecting an increasing chemical complexity. The results are decisive. While data augmentation reduces the error of the baseline GRACE-FS-M, its performance plateaus at a level inferior to GRACE-2L. This proves that the limitation of GRACE-FS-M is not a simple lack of data

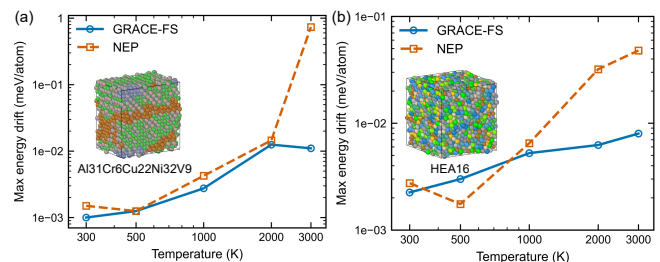


FIG. 5. Assessing the thermal stability of HEAs via MD simulations. The maximum energy drift, a key metric for stability, is plotted for (a) the $\text{Al}_{31}\text{Cr}_6\text{Cu}_{22}\text{Ni}_{32}\text{V}_9$ alloy with chemical short-range order (CSRO) and (b) a random 16-element alloy across a range of temperatures.

but is inherent to its architectural design, which fundamentally constrains its ability to capture complex, multi-element interactions. Therefore, the superior performance of GRACE-2L, achieved without any multicomponent training data, delivers a powerful insight: for the prediction of complex multicomponent systems, a sophisticated model architecture is not just beneficial, but is a prerequisite for achieving high-fidelity extrapolation, outweighing the benefits of targeted data expansion.

Validation of MLIPs for key properties

We next evaluate the accuracy of the MLIPs in predicting key mechanical properties of pure metals, with all reference DFT data obtained from Ref. [31]. Figure 7(a) presents a parity plot of the elastic constants for 16 metals. All MLIPs capture the general trends well, with GRACE-FS-M and UNEP-v1 showing comparable errors. The augmented GRACE-FS-M-A model, however, demonstrates a marked reduction in error. For more localized defects, the advantages of the GRACE models become more pronounced. As shown in Fig. 7(b, c), GRACE-FS-M provides a more accurate prediction of both the monovacancy formation energy and surface energy than UNEP-v1. Furthermore, data augmentation yields consistent improvements, with GRACE-FS-M-A achieving the highest accuracy. Finally, we probe the complex energy landscape of a screw dislocation in BCC tungsten (W) (Fig. 7(d)). While the UNEP-v1 model underestimates the Peierls barrier, the GRACE-FS models slightly overestimate it; critically, all models yield results close to the DFT reference.

These results collectively demonstrate two key findings: first, the GRACE-FS-M architecture inherently provides superior accuracy for mechanical property prediction, particularly for defect properties, compared to UNEP-v1. Second, the systematic use of data augmentation (GRACE-FS-M-A) consistently enhances accuracy,

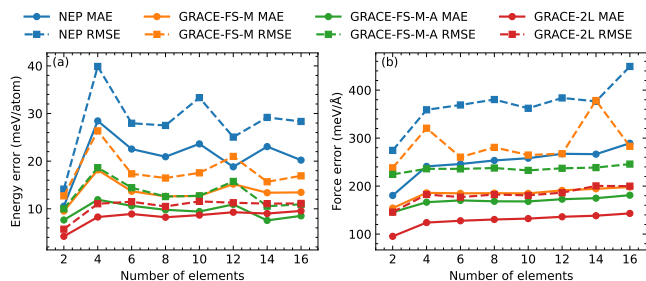


FIG. 6. Assessing the chemical transferability of different MLIPs. Prediction errors for (a) energy and (b) forces (reported as MAE and RMSE) are evaluated on additional DFT datasets of multi-element systems, ranging from 2 to 16 components.

even for properties not explicitly included in the augmented dataset. This indicates that the augmented data broadens the model’s foundational understanding of the potential energy surface, leading to more robust and transferable predictions.

A key validation of the MLIPs involves their application to the finite-temperature deformation of complex, multicomponent systems. For this purpose, we subject two representative high-entropy alloys (HEAs), a FCC Ni-Cu-Pd-Pt-Ag-Au alloy and a BCC V-Cr-Mo-Ta-W-Ti alloy, to tensile loading at a strain rate of 10^9 s^{-1} up to 35% strain. The resultant defect evolution, analyzed via common neighbor analysis (Fig. 8(a, b)), reveals distinct, complex deformation mechanisms. The FCC HEA undergoes a series of phase transformations from FCC to BCC and HCP structures, accompanied by the formation of unidentified defects. In contrast, the BCC HEA experiences severe plastic deformation, generating a high density of defects and forming systemic boundaries at the maximum strain. The ability to capture such intricate behavior provides a stringent validation for the MLIPs. As shown in Fig. 8(c, d), the GRACE-FS models achieve significantly lower energy and force errors than UNEP-v1 for both HEAs. Furthermore, all potentials exhibit higher accuracy in the FCC structure than in the BCC structure. These results collectively demonstrate that the GRACE-FS architecture provides a more robust and reliable framework for simulating the mechanical response of chemically complex systems, with a particular advantage in capturing the challenging deformation pathways of BCC alloys.

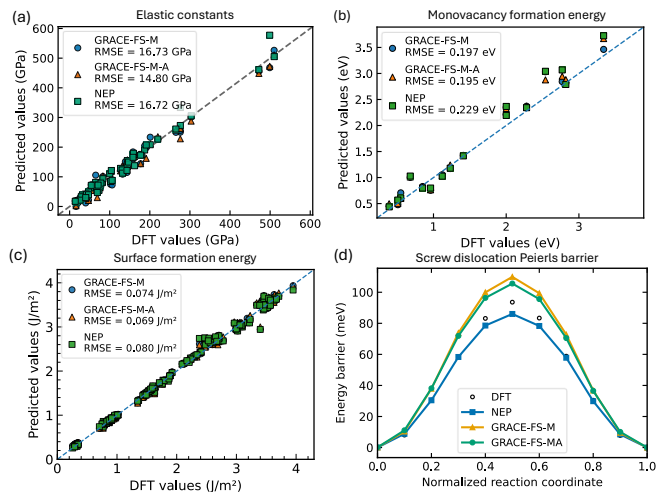


FIG. 7. Assessment of MLIP accuracy in predicting fundamental mechanical properties. The MLIP-predicted (a) elastic constants, (b) vacancy formation energy, (c) surface energy, and (d) screw dislocation Peierls barrier are plotted against their respective DFT values.

Shock simulations and uncertainty analysis

We next employ the UNEP-v1 ensemble to investigate the shock response of the high-entropy alloy $\text{Al}_{10}\text{Cr}_{10}\text{Cu}_{35}\text{Ni}_{35}\text{V}_{10}$ via non-equilibrium MD (NEMD) simulations. The simulation cell, containing 3 million atoms with dimensions of $18 \times 18 \times 110 \text{ nm}^3$, is subjected to an impact velocity of 0.8 km/s along the [100] crystallographic direction. The shock loading is applied for 10.0 ps using the “ensemble wall_mirror” method in the GPUMD package [44], followed by a 35.0 ps relaxation period to observe subsequent deformation and failure mechanisms. Owing to their high computational demand, GRACE-FS potentials are deemed unsuitable for such application.

Figure 9(a-c) presents the evolution of density, stress, and temperature during the shock process, as simulated by the primary UNEP-v1 model from Ref. [31]. The UNEP-v1 model properly captures the dynamic response of these quantities throughout both the shock compression and release stages, including wave propagation, reflection, and interaction. A spall fracture is initiated at approximately 30 ps, marked by a sharp drop in density (Fig. 9(a)) and a concurrent temperature increase (Fig. 9(c)). The spall strength, defined as the maximum tensile stress experienced by the material, is determined to be 16.69 GPa for this primary model. To assess model uncertainty, the spall strength was calculated using four additional UNEP-v1 models from the ensemble, yielding values of 17.07, 17.70, 17.47, and 16.76 GPa. The standard deviation across all five models is 0.39 GPa, representing an uncertainty of only $\sim 2.3\%$ relative to the mean value of 17.14 GPa. This low uncertainty confirms the re-

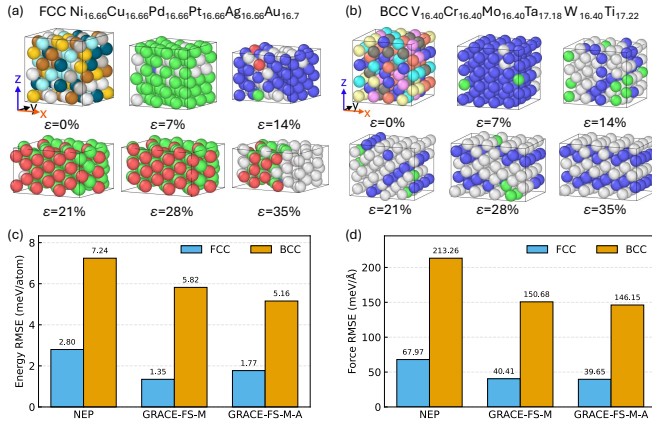


FIG. 8. Performance evaluation of MLIPs for simulating the tensile testing of HEAs. (a, b) Snapshots of defect structures (e.g., phase transitions, stacking faults) during deformation for FCC and BCC crystal structures, respectively. (c, d) The accuracy of the MLIPs is quantified by RMSE for (c) energy and (d) force predictions compared to reference DFT calculations.

liability of the UNEP-v1 ensemble for determining spall strength via NEMD simulations. In contrast, Fig. 9(d-f) shows the spatial distributions of these quantities at the simulation end time (45 ps) for all five UNEP-v1 models. These snapshots reveal non-negligible deviations in critical regions, particularly in the density and temperature profiles within the spall zone.

We next analyze the microstructure evolution and failure mechanisms. Figure 10(a) presents the sequence from the main UNEP-v1 model. By the end of the shock stage (10 ps), a dense dislocation network has formed. Subsequently, void nucleation occurs at the right end of the sample by 30 ps, leading to complete fracture into two parts by 45 ps. The temporal evolution of the total dislocation length across the five-model UNEP-v1 ensemble is shown in Fig. 10(b). All models exhibit a consistent trend: a sharp increase in dislocation density occurs before 10 ps, followed by a plateau between 10-18 ps. A rapid decrease then follows, nearly vanishing by 26 ps. Beyond 30 ps, the dislocation length increases once more, peaking around 34 ps before declining again. Despite this qualitative agreement, significant quantitative deviations are observed between the models, particularly during the 10-18 ps plateau, where the maximum dislocation length varies considerably. This variability in microstructural evolution underlies the spatial deviations in temperature and density observed in the spall region in Fig. 9(d-f), highlighting that while the global spall strength is robust, the local damage microstructure is more model-sensitive.

DISCUSSION

MLIPs enable near-DFT accuracy at orders-of-magnitude lower cost, a capability that is especially valuable for high-entropy materials, where multicomponent

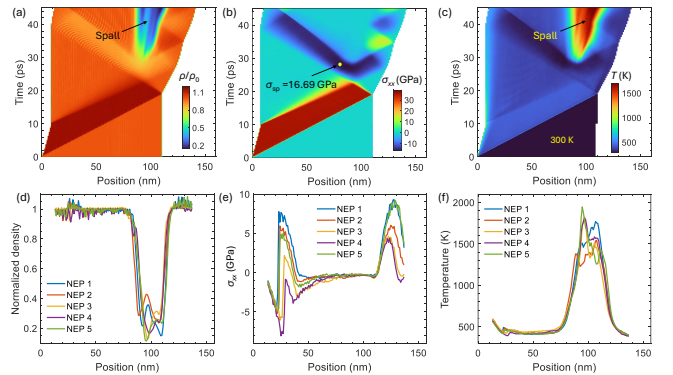


FIG. 9. Shock-induced spallation in $\text{Al}_{10}\text{Cr}_{10}\text{Cu}_{35}\text{Ni}_{35}\text{V}_{10}$. Temporal evolution of (a) density, (b) stress, and (c) temperature from the primary UNEP-v1 model. The arrows indicate the spallation, and the calculated spall strength (σ_{sp}) is marked in (b). Corresponding spatial profiles of (d) density, (e) stress, and (f) temperature at 45 ps, comparing results across the five-model UNEP-v1 ensemble.

chemistry and complex interactions govern defect formation and evolution. In this work, we conducted a comprehensive head-to-head assessment of two MLIPs, UNEP-v1 and GRACE-FS, that are designed to handle arbitrary elemental combinations and scale to million-atom simulations. Using a carefully curated DFT dataset spanning 16 elemental metals and their binaries, we systematically evaluated their accuracy, robustness, and scalability.

Our comparative analysis reveals a clear trade-off between computational throughput and predictive accuracy. The UNEP-v1 model demonstrates a decisive advantage in inference speed, being approximately 40 times faster than the GRACE-FS framework for large-scale MD simulations. This makes NEP uniquely suited for extensive sampling or simulating very large systems (e.g., millions of atoms) where computational cost is the primary constraint. However, this speed comes with compromises: GRACE-FS achieves better accuracy in predicting mechanical properties, exhibits enhanced stability in high-temperature MD simulations, and possesses significantly better chemical extrapolation capabilities. Furthermore, the training speed of UNEP-v1 is notably slower, making it less practical for on-the-fly active learning workflows. Therefore, for simulations where system size or resource constraints are not prohibitive, GRACE-FS is the recommended choice due to its robust all-around performance. Conversely, UNEP-v1 is strongly recommended for applications where simulation speed is the paramount concern and a slight decrease in accuracy is acceptable.

On the other hand, our results also have important implications for developing MLIPs for multicomponent systems, such as high-entropy alloys, ceramics, and 2D materials. Previous work has suggested that training on only unary and binary structures can already provide a reasonable description for high-entropy alloys [31], and our results partly support this view: the unary-plus-binary strategy is indeed effective as a practical starting point, because it substantially reduces the chemical-

composition space while still yielding a nontrivial level of accuracy. In this sense, such a dataset construction strategy can serve as an efficient foundation for MLIP development in complex chemical systems. However, Fig. 6 also reveals a systematic reduction in accuracy for systems containing three or more elements, indicating that unary and binary data alone are generally insufficient to guarantee robust performance in truly multi-element environments. Therefore, while the unary-plus-binary strategy is valuable for narrowing the chemical space and building an initial model, the inclusion of ternary or higher-order configurations remains crucial for achieving better transferability and reliability in realistic multicomponent applications. At the same time, the extent to which such higher-order training data are required differs across MLIP architectures, reflecting their different chemical extrapolation capabilities. Fig. 6 shows a clear hierarchy in this regard: the GRACE-2L potential outperforms GRACE-FS, which in turn surpasses NEP. Consequently, the necessary composition and complexity of the DFT dataset depend on the chosen MLIP architecture. More advanced potential frameworks can alleviate, although not completely remove, the need for exhaustive multi-element training data. This conclusion is consistent with the recent emergence of universal MLIPs, such as MACE and eqV2, whose more expressive architectures enable near-DFT accuracy across broad compositional spaces, in some cases even without system-specific fine-tuning [45].

Finally, it is important to emphasize the distinct advantages of the NEP framework. The primary limitation of NEP is its slow training speed, a challenge that future work on gradient-based training algorithms could potentially address [46]. Despite this, NEP’s performance within GPUMD for large-scale MD is exceptional. Its key strength lies in its superior computational efficiency, which provides researchers with critical flexibility: they can achieve longer simulation timescales, model larger system sizes, or employ more physically accurate (slower) strain rates. Furthermore, its coverage of common metallic elements makes it a highly accessible and valuable tool for the materials science and mechanics communities. Our shock simulations of a prototypical FCC high-entropy alloy demonstrate NEP’s practical reliability: the uncertainty in the calculated spall strength is remarkably small, and the evolution of key quantities and microstructural failure mechanisms are consistently captured across the model ensemble. This positions NEP as a promising and robust tool for modeling complex materials under extreme loading conditions.

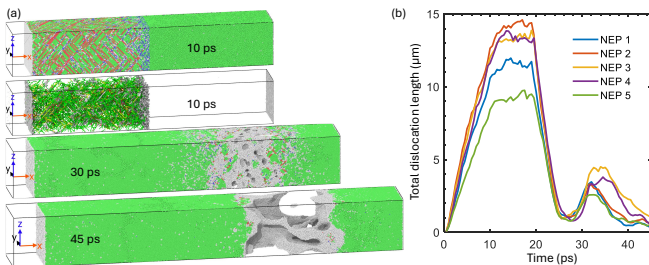


FIG. 10. Microstructural evolution during shock simulation. (a) Defect formation at different times. The first panel visualizes dislocation lines via the Dislocation Extraction Algorithm (DXA), while the subsequent panels show defects identified by Common Neighbor Analysis (CNA). (b) Temporal evolution of the total dislocation length for five different UNEP-v1 models.

CONCLUSION

In summary, this work presents a rigorous benchmark of the NEP and GRACE-FS MLIP frameworks for mul-

ticomponent systems. We have demonstrated that while GRACE-FS offers advantages in training speed and extrapolation, NEP provides a critical balance of accuracy and exceptional computational efficiency for large-scale MD simulations. The successful application of the NEP ensemble to model the complex process of shock-induced spallation in a high-entropy alloy, yielding robust predictions with quantifiable uncertainty, underscores its maturity and reliability. These findings provide clear guidelines for potential users and mark a significant step toward the reliable simulation of complex materials under extreme conditions.

DATA AVAILABILITY

All the GRACE-FS, GRACE-2L models and validation DFT dataset for multicomponent alloys are available at <https://doi.org/10.5281/zenodo.19187064>.

ACKNOWLEDGMENTS

This work was sponsored by Nederlandse Organisatie voor Wetenschappelijk Onderzoek (The Netherlands Organization for Scientific Research, NWO) domain Science for the use of supercomputer facilities. The authors also acknowledge the use of DelftBlue supercomputer, provided by Delft High Performance Computing Center (<https://www.tudelft.nl/dhpc>). This work was supported by the National Outstanding Youth Science Fund Project (number 12125206), Major International Joint Research Projects (number W2411003) of NSFC.

-
- [1] Y. Cao, K. Sheriff, and R. Freitas, Capturing short-range order in high-entropy alloys with machine learning potentials, *npj Computational Materials* **11**, 10.1038/s41524-025-01722-2 (2025).
- [2] H. Meng, Y. Liu, H. Yu, L. Zhuang, and Y. Chu, Machine-learning-potential-driven prediction of high-entropy ceramics with ultra-high melting points, *Cell Reports Physical Science* **6**, 102449 (2025).
- [3] J. Behler and M. Parrinello, Generalized neural-network representation of high-dimensional potential-energy surfaces, *Physical Review Letters* **98**, 10.1103/physrevlett.98.146401 (2007).
- [4] A. P. Bartók, M. C. Payne, R. Kondor, and G. Csányi, Gaussian approximation potentials: The accuracy of quantum mechanics, without the electrons, *Physical Review Letters* **104**, 10.1103/physrevlett.104.136403 (2010).
- [5] I. S. Novikov, K. Gubaev, E. V. Podryabinkin, and A. V. Shapeev, The mlip package: moment tensor potentials with mpi and active learning, *Machine Learning: Science and Technology* **2**, 025002 (2021).
- [6] R. Drautz, Atomic cluster expansion for accurate and transferable interatomic potentials, *Physical Review B* **99**, 014104 (2019).
- [7] X.-y. Meng, L. Zhang, H.-y. Wang, and L.-h. Dai, Atomistic mechanism underlying shock-induced phase transition in hfnbtatizr energetic high-entropy alloy, *Energetic Materials Frontiers* **6**, 103–111 (2025).
- [8] B. Deng, P. Zhong, K. Jun, J. Riebesell, K. Han, C. J. Bartel, and G. Ceder, Chgnet as a pretrained universal neural network potential for charge-informed atomistic modelling, *Nature Machine Intelligence* **5**, 1031 (2023).
- [9] Y.-L. Liao, B. Wood, A. Das, and T. Smidt, Equiformerv2: Improved equivariant transformer for scaling to higher-degree representations, *arXiv preprint arXiv:2306.12059* (2023).
- [10] Y. Park, J. Kim, S. Hwang, and S. Han, Scalable parallel algorithm for graph neural network interatomic potentials in molecular dynamics simulations, *J. Chem. Theory Comput.* **20**, 4857 (2024).
- [11] M. Neumann, J. Gin, B. Rhodes, S. Bennett, Z. Li, H. Choubisa, A. Hussey, and J. Godwin, Orb: A fast, scalable neural network potential, *arXiv preprint arXiv:2410.22570* (2024).
- [12] D. Wines and K. Choudhary, Chips-ff: Evaluating universal machine learning force fields for material properties, *ACS Materials Letters* **7**, 2105–2114 (2025).
- [13] B. M. Wood, M. Dzamba, X. Fu, M. Gao, M. Shuaibi, L. Barroso-Luque, K. Abdelmaqsoud, V. Gharakhanyan, J. R. Kitchin, D. S. Levine, K. Michel, A. Sriram, T. Cohen, A. Das, A. Rizvi, S. J. Sahoo, Z. W. Ulissi, and C. L. Zitnick, Uma: A family of universal models for atoms (2026), *arXiv:2506.23971 [cs.LG]*.
- [14] Z. Fan, Z. Zeng, C. Zhang, Y. Wang, K. Song, H. Dong, Y. Chen, and T. Ala-Nissila, Neuroevolution machine learning potentials: Combining high accuracy and low cost in atomistic simulations and application to heat transport, *Physical Review B* **104**, 104309 (2021).
- [15] K. Xu, H. Bu, S. Pan, E. Lindgren, Y. Wu, Y. Wang, J. Liu, K. Song, B. Xu, Y. Li, T. Hainer, L. Svensson, J. Wiktor, R. Zhao, H. Huang, C. Qian, S. Zhang, Z. Zeng, B. Zhang, B. Tang, Y. Xiao, Z. Yan, J. Shi, Z. Liang, J. Wang, T. Liang, S. Cao, Y. Wang, P. Ying, N. Xu, C. Chen, Y. Zhang, Z. Chen, X. Wu, W. Jiang, E. Berger, Y. Li, S. Chen, A. J. Gabourie, H. Dong, S. Xiong, N. Wei, Y. Chen, J. Xu, F. Ding, Z. Sun, T. Ala-Nissila, A. Harju, J. Zheng, P. Guan, P. Erhart, J. Sun, W. Ouyang, Y. Su, and Z. Fan, Gpumd 4.0: A high-performance molecular dynamics package for versatile materials simulations with machine-learned potentials, *Materials Genome Engineering Advances* **3**, 10.1002/mgea.70028 (2025).
- [16] H. Dong, Y. Shi, P. Ying, K. Xu, T. Liang, Y. Wang, Z. Zeng, X. Wu, W. Zhou, S. Xiong, *et al.*, Molecular dynamics simulations of heat transport using machine-learned potentials: A mini-review and tutorial on gpumd with neuroevolution potentials, *Journal of Applied Physics* **135** (2024).
- [17] P. Ying, W. Zhou, L. Svensson, E. Berger, E. Fransson, F. Eriksson, K. Xu, T. Liang, J. Xu, B. Song, *et al.*, Highly efficient path-integral molecular dynamics simulations with gpumd using neuroevolution potentials: Case studies on thermal properties of materials, *The Journal of Chemical Physics* **162** (2025).

- [18] T. Liang, K. Xu, E. Lindgren, Z. Chen, R. Zhao, J. Liu, E. Berger, B. Tang, B. Zhang, Y. Wang, K. Song, P. Ying, N. Xu, H. Dong, S. Chen, P. Erhart, Z. Fan, T. AlaNissila, and J. Xu, Nep89: Universal neuroevolution potential for inorganic and organic materials across 89 elements (2025).
- [19] A. Bochkarev, Y. Lysogorskiy, and R. Drautz, Graph atomic cluster expansion for semilocal interactions beyond equivariant message passing, *Phys. Rev. X* **14**, 021036 (2024).
- [20] L. Barroso-Luque, M. Shuaibi, X. Fu, B. M. Wood, M. Dzamba, M. Gao, A. Rizvi, C. L. Zitnick, and Z. W. Ulissi, Open materials 2024 (omat24) inorganic materials dataset and models (2024), arXiv:2410.12771 [condmat.mtrl-sci].
- [21] J. Schmidt, N. Hoffmann, H. Wang, P. Borlido, P. J. M. A. Carriço, T. F. T. Cerqueira, S. Botti, and M. A. L. Marques, Machine-learning-assisted determination of the global zero-temperature phase diagram of materials, *Advanced Materials* **35**, 10.1002/adma.202210788 (2023).
- [22] Y. Lysogorskiy, A. Bochkarev, and R. Drautz, Graph atomic cluster expansion for foundational machine learning interatomic potentials, *npj Computational Materials* 10.1038/s41524-026-01979-1 (2026).
- [23] A. P. Thompson, H. M. Aktulga, R. Berger, D. S. Bolinteanu, W. M. Brown, P. S. Crozier, P. J. in 't Veld, A. Kohlmeyer, S. G. Moore, T. D. Nguyen, R. Shan, M. J. Stevens, J. Tranchida, C. Trott, and S. J. Plimpton, LAMMPS - a flexible simulation tool for particle-based materials modeling at the atomic, meso, and continuum scales, *Comp. Phys. Comm.* **271**, 108171 (2022).
- [24] S. Zhao, G. M. Stocks, and Y. Zhang, Stacking fault energies of face-centered cubic concentrated solid solution alloys, *Acta Materialia* **134**, 334 (2017).
- [25] X. Chen, Q. Wang, Z. Cheng, M. Zhu, H. Zhou, P. Jiang, L. Zhou, Q. Xue, F. Yuan, J. Zhu, *et al.*, Direct observation of chemical short-range order in a medium-entropy alloy, *Nature* **592**, 712 (2021).
- [26] P. Cao, Maximum strength and dislocation patterning in multi-principal element alloys, *Science advances* **8**, eabq7433 (2022).
- [27] S. K. Nemani, M. Torkamanzadeh, B. C. Wyatt, V. Presser, and B. Anasori, Functional two-dimensional high-entropy materials, *Communications Materials* **4**, 16 (2023).
- [28] R.-Z. Zhang and M. J. Reece, Review of high entropy ceramics: design, synthesis, structure and properties, *Journal of Materials Chemistry A* **7**, 22148 (2019).
- [29] X. Zhou, J. Marian, F. Zhou, and V. V. Bulatov, Probing multi-dimensional composition spaces in search of strong metallic alloys, *npj Computational Materials* (2026).
- [30] L. A. Zepeda-Ruiz, A. Stukowski, T. Opperstrup, and V. V. Bulatov, Probing the limits of metal plasticity with molecular dynamics simulations, *Nature* **550**, 492 (2017).
- [31] K. Song, R. Zhao, J. Liu, Y. Wang, E. Lindgren, Y. Wang, S. Chen, K. Xu, T. Liang, P. Ying, *et al.*, General-purpose machine-learned potential for 16 elemental metals and their alloys, *Nature Communications* **15**, 10208 (2024).
- [32] G. Kresse and J. Furthmüller, Efficient iterative schemes for ab initio total-energy calculations using a plane-wave basis set, *Physical Review B* **54**, 11169–11186 (1996).
- [33] J. P. Perdew, K. Burke, and M. Ernzerhof, Generalized gradient approximation made simple, *Physical Review Letters* **77**, 3865–3868 (1996).
- [34] P. E. Blöchl, Projector augmented-wave method, *Physical Review B* **50**, 17953–17979 (1994).
- [35] V. Wang, N. Xu, J.-C. Liu, G. Tang, and W.-T. Geng, Vaspkit: A user-friendly interface facilitating high-throughput computing and analysis using vasp code, *Computer Physics Communications* **267**, 108033 (2021).
- [36] Z. Fan, Dataset for UNEP-v1, 10.5281/zenodo.11533864 (2024).
- [37] J. F. Ziegler and J. P. Biersack, The stopping and range of ions in matter, in *Treatise on Heavy-Ion Science: Volume 6: Astrophysics, Chemistry, and Condensed Matter*, edited by D. A. Bromley (Springer US, Boston, MA, 1985) pp. 93–129.
- [38] Y. Lysogorskiy, A. Bochkarev, M. Mrovec, and R. Drautz, Active learning strategies for atomic cluster expansion models, *Physical Review Materials* **7**, 043801 (2023).
- [39] E. V. Podryabinkin and A. V. Shapeev, Active learning of linearly parametrized interatomic potentials, *Computational Materials Science* **140**, 171 (2017).
- [40] https://github.com/psn417/nep_extrapolation.
- [41] A. Stukowski, Visualization and analysis of atomistic simulation data with ovito—the open visualization tool, *Modelling and Simulation in Materials Science and Engineering* **18**, 015012 (2009).
- [42] F. Shuang, Z. Wei, K. Liu, W. Gao, and P. Dey, Model accuracy and data heterogeneity shape uncertainty quantification in machine learning interatomic potentials, *Machine Learning: Science and Technology* **7**, 025002 (2026).
- [43] N. Leimeroth, L. C. Erhard, K. Albe, and J. Rohrer, Machine-learning interatomic potentials from a users perspective: a comparison of accuracy, speed and data efficiency, *Modelling and Simulation in Materials Science and Engineering* **33**, 065012 (2025).
- [44] S. Pan, J. Shi, Z. Liang, C. Liu, J. Wang, Y. Wang, H.-T. Wang, D. Xing, and J. Sun, Shock compression pathways to pyrite silica from machine learning simulations, *Physical Review B* **110**, 10.1103/physrevb.110.224101 (2024).
- [45] F. Shuang, Z. Wei, K. Liu, W. Gao, and P. Dey, Universal machine learning interatomic potentials poised to supplant dft in modeling general defects in metals and random alloys, *Machine Learning: Science and Technology* **6**, 030501 (2025).
- [46] H. Huang, J. Peng, K. Li, J. Zhou, and Z. Sun, Efficient gpu-accelerated training of a neuroevolution potential with analytical gradients, *Computer Physics Communications* **320**, 109994 (2026).